Modeling Power Losses in Electric Vehicle BLDC Motor

James Kuria[1*] Pyung Hwang[2]

1. Department of Mechanical Engineering, Jomo Kenyatta University of Agriculture and Technology, P.O. Box 62000-00200, Nairobi, Kenya

2. School of Mechanical Engineering, Yeungnam University, Gyeongsan, 712-749, Republic of Korea

* E-mail of the corresponding author: jkuria@eng.jkuat.ac.ke

Abstract

In order to design an efficient motor cooling system, it is important to accurately predict the power losses which are normally dissipated in form of heat. This study presents an analytical method for estimating bearing frictional losses and numerical method for estimating electromagnetic losses for an electric vehicle BLDC motor. The power losses obtained are used as heat sources when evaluating the thermal performance of the motor. The results showed that electromagnetic losses are dominant and contribute over 80% of all losses, while bearing losses contribute about 12% of the total electric motor. The results also showed that bearing losses increase significantly with increasing speed or load.

Keywords: BLDC motor, bearing frictional losses, electromagnetic losses, joules losses, eddy current losses

1. Introduction

Extensive research on electric vehicle motor system is currently being conducted to minimize overreliance on petroleum products and to curb emissions associated with climate change. When designing an electric motor, it is important to study the motor losses in order to find ways of improving motor efficiency and to design an efficient cooling system. Motor losses consist of electromagnetic and mechanical losses.

The electromagnetic losses have been well understood since most electric motor designers have an electrical background. Kyoung-Jin et al (Ko et al., 2010), undertook a study to predict electromagnetic losses of a high speed permanent magnet synchronous motor using analytical and FEA. Coupled electromagnetic and thermal studies have been carried by various researchers (Driesen et al., 2002; Marignetti, 2007; Z. Makni, 2007; Dorell, 2008). In most of these studies, the effect of mechanical losses was neglected or expressed using a factor. However, to accurately predict the overall efficiency and total heat generated in a motor system, the mechanical losses, which include bearing and windage losses, have to be considered. This work aims at investigating the electromagnetic and mechanical power losses of a 1.2 kW brushless direct current (BLDC) permanent magnet motor. The specifications of the motor are shown in Table 1. The motor is to be used to power an electric vehicle compressor.

2. Bearing Frictional Losses

Bearing friction losses consist of four main components (Hamrock & Anderson, 1983):
1. Hydrodynamic rolling force.
2. Sliding friction losses between the rolling elements and the races.
3. Sliding friction between the rolling elements and the separator/ cage.
4. Hysteresis losses.

2.1 Forces on Ball-Race Contacts

The tangential forces acting on a ball-race contact can be evaluated from Figure 1. The following forces act between the ball and the outer race: hydrodynamic rolling forces, FR_o and friction forces Fs_o. Also, between the ball and the inner race act the following forces: hydrodynamic rolling forces, FR_i and friction forces Fs_i. Between the ball and the cage, act normal force FB.

2.2 Hydrodynamic Rolling Force

The hydrodynamic rolling force is due to the Poiseuille flow or pressure gradient in the inlet of an elastohydrodynamic lubrication (EHL) contact and is responsible for the hydrodynamic race torque, even when operating under pure rolling conditions. In the EHL condition, this force can be approximated by the relationship (Houpert, 1999):

$$F_R = 2.86 \cdot E' \cdot R_x^2 \cdot k^{0.348} \cdot G^{0.022} \cdot U^{0.66} \cdot W^{0.47} \tag{1}$$

where G, U and W are dimensionless material, speed and load parameters, R_x is the equivalent radius in the rolling direction, E' is equivalent Young's modulus and k is radius ratio.

2.3 Sliding Frictional Forces

The friction forces Fs_i and Fs_o on the two contacts are the sliding traction forces due to microslip occurring in the contact. This force can be computed from shear stresses on the contact ellipse (Houpert, 1999). Since the variation of shear stress on the contact ellipse is a complex problem, these forces can be computed from equilibrium of forces and moments acting on the ball (Figure 1 and 2)

The resulting sliding forces are given by:

$$Fs_i = \frac{MC_o + MC_i + MER_o + MER_i + MB}{d_w} + FR_o + \frac{(FR_i + FR_o) d_w \cos\cos\alpha}{d_m} + \frac{FB}{2} \tag{2}$$

$$Fs_i = \frac{MC_o + MC_i + MER_o + MER_i + MB}{d_w} + FR_o - \frac{(FR_i + FR_o) d_w \cos\cos\alpha}{d_m} - \frac{FB}{2} \tag{3}$$

The coefficient of friction in the ball-race system depends on the lubrication regime, whether limited, mixed or full EHL. In this study, methods of Hamrock (Hamrock, 1994) were used to determine the coefficient of friction based on the lubrication regime.

2.4 Frictional Torque Developed in Ball-Race Contacts

From Figure 1, the total tangential force, F_i, F_o, between the ball and races can be determined by taking the algebraic sum of the contact forces in the rolling direction.

$$F_i = FR_i + Fs_i \tag{4}$$

$$F_o = FR_o + Fs_o \tag{5}$$

The friction torque developed between a ball and outer race contact is:

$$M_i = F_i \cdot R_i \qquad (6)$$

$$M_o = F_o \cdot R_o \qquad (7)$$

Where R_i and R_o are the radius of ball-inner race and ball-outer race contacts respectively.

For z loaded balls, the total friction torque acting on the bearing is obtained by summing all the friction torques in the ball-race contacts:

$$MI = \sum_{j=1}^{z} M_{i,j} \qquad (8)$$

$$MI = \sum_{j=1}^{z} M_{o,j} \qquad (9)$$

2.5 Bearing Frictional Power Losses

The friction power loss from the bearing can be approximated by the product of the friction torque and the orbital velocity of the balls, ω_c. Thus,

$$P = [MI + MO]\omega_c \qquad (10)$$

The above set of equations is applied to individual bearings depending on the number of bearings in the motor system.

The equations formulated in the study were coded into a FORTRAN program and simulated. An IPM motor mounted between two ball bearings was analyzed in the study. The bearing reaction with a dynamic factor was taken to as the bearing radial load. Table 2 shows the specifications of a deep groove bearing used in the analysis. General purpose bearing lubricant was used in the analysis (SKF, 2009).

3. Electromagnetic Losses

Electromagnetic losses consist of two main components:

    I. Winding copper losses P_{cu} that are caused by resistive heating of the copper windings and are defined by:

$$P_{cu} = 3R_\theta I_{rms}^2 \qquad (11)$$

where R_θ and I_{rms} are respectively the winding phase resistance and the RMS value of the motor phase current.

II. Core losses P_{fe}, consist of eddy current losses and hysteresis effect. In brushless DC motors, the variation of flux in the stator core is not sinusoidal and hence the iron core loss is given by:

$$P_{fe} = k_h f \hat{B}^\alpha + \frac{k_e}{2\pi^2}\left\{\frac{dB}{dt}\right\}_{rms}^2 \text{ (W/kg)} \tag{12}$$

Where the first term is the hysteresis loss and the second is the eddy current loss. $\hat{B}$ is the peak value of the flux density and f, k_h, α and k_e are constants determined by curve fitting from manufacturer's data (Andrada et al., 2004).

The electromagnetic losses were obtained using Ansoft Maxwell that e mploys finite element analysis. Due to periodicity of the motor, only ¼ of the motor was analyzed in order to reduce the computational requirements. Figure 3 shows the 2D FEA mesh of ¼ of the motor used in the study.

4. Results and Discussions
The results obtained in the above analyses are presented and discussed in this section.

4.1 Bearing Losses

Generally, the load on a rolling element varies within the load distribution zone. Methods by Brian and Robert (Holm-Hansen & Gao, 2000) were employed to determine the load distribution on a rolling element. Figure 4 shows variation of the contact load on a rolling element.

Figure 5 shows the variation of hydrodynamic rolling force and sliding friction force on a rolling element with the contact angle. It is evident that the load distribution influences the contact forces on the rolling element as the shape of the curves is similar to that of the load distribution.

Figure 6 shows the variation of the total bearing loss as a function of angular displacement. The fluctuations of the loss are due to the change in the number of rolling elements within the load carrying zone.

Figure 7 shows variation of frictional torque with speed which shows that the frictional torque increases with speed. Figure 8 shows variation of power loss with speed. When a motor system is to operate at high speeds, then the bearing frictional losses cannot be neglected (Dorell, 2008).

4.2 Electromagnetic Losses
Figure 9 shows contour plots of the core loss obtained from MAXWELL simulations.

Figure 10 and 11 show transient core and stranded copper losses respectively. The core loss is dependent on rotor and stator material properties while stranded loss is directly proportional to the current density. Stranded windings were employed in the analysis in order to simplify the computations.

Table 3 shows the various motor losses and corresponding heat sources computed for the BLDC motor in this study. These heat sources can be used in designing an efficient cooling system for the motor.

5. Conclusion

The analysis showed that electromagnetic losses are dominant and contribute over 80% of all motor losses, while bearing losses contribute about 12% of the total motor losses. The major contribution to the bearing losses is the sliding friction due to microslip occurring at the ball-race contacts. This results show that it is imperative that bearing losses should be included when quantifying motor losses to estimate motor efficiency and in the design of efficient cooling systems for the motor.

References

Ko, K.-J., Jang, S.-M., Park, J.-H., & Lee, S.-H. (2010). Electromagnetic losses calculation of 5kW class high speed permanent magnet synchronous motor considering current waveform. *IEEE Transactions on Industry Applications*.

Driesen, J., Belmans, J. M., & Hameyer, K. (2002). Methodologies for coupled transient electromagnetic-therma finite element modeling of electrical energy transducers. *IEEE Transactions on Industry Applications, 38*(5), 12441250.

Marignetti, F. (2007). *Coupled electro magnetic thermal and fluid dynamical simulation of axial flux PM synchronous machines.* Paper presented at the COMSOL Users Conference, Grenoble.

Z. Makni, M. B. a. C. M. (2007). A coupled electromagnetic-thermal model for the design of electrical machines. *The International Journal for Computation and Mathematics in Electrical and Electronic Engineering, 26*(1), 201-213.

Dorell, D. G. (2008). Combined Thermal and Electromagnetic Analysis of Permanent-Magnet and Induction Machines to Aid Calculation. *IEEE Transactions on Industry Applications, 55*(10), 3566-3574.

Hamrock, B. J., & Anderson, W. J. (1983). Rolling - Element Bearing: National Aeronautics and Space Administration (NASA).

Houpert, L. (1999). *Numerical and Analytical Calculations in Ball Bearings.* Paper presented at the Congres Roulements.

Hamrock, B. J. (1994). *Fundamentals of Fluid Film Lubrication* (International ed.): McGrawHill, Inc.

SKF, G. (2009). SKF General Purpose Industrial and Automotive Grease: SKF Group.

Andrada, P., Torrent, M., Perat, J. I., & Blanque, B. (2004). Power Losses in Outside-Spin Brushless D.C. Motors: Universitat Politecnica de Catalunya.

Holm-Hansen, B. T., & Gao, R. X. (2000). Vibration Analysis of a Sensor-Integrated Ball Bearing. *Transactions of the ASME, 122*, 384-392.

Table 1. Motor properties.

Parameter	Value
Type	BLDC PM motor
Power rating	1.2 kW
Maximum speed	13,000 rpm
Rated speed	8,000 rpm

Rated torque	1.5 Nm
Voltage	DC 72 V
Housing diameter	120 mm

Table 2. Dimensions of a deep groove ball bearing (Bearing No. 6004) (SKF, 2009).

Parameter	Value
Outer diameter	42 mm
Bore diameter	20 mm
Ball diameter	6.35 mm
Raceway width	12 mm
Contact angle	0°
Load distribution factor	0.45
No. of rolling elements	13

Table 3. Motor losses and corresponding heat sources.

Loss	Value	Heat source (W/m^3)	
Coreloss	50 W	Stator teeth	114,800
		Stator tip	800,000
		Stator body	1,600,000
		Rotor	114,800
Copper losses	150 W		3,000,000
Bearing friction loss	12 W		450,000
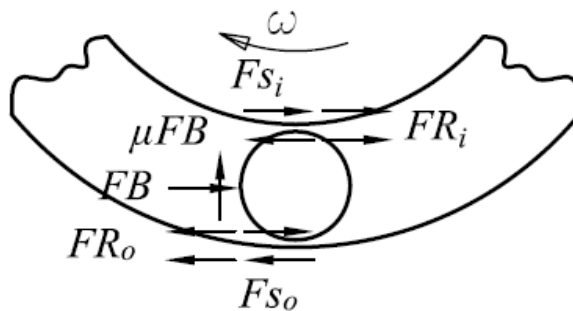
Figure 1. Forces acting on a ball and the two races of a ball bearing system.

Journal of Energy Technologies and Policy
www.iiste.org
ISSN 2224-3232 (Paper)   ISSN 2225-0573 (Online)
Vol.1, No.4, 2011
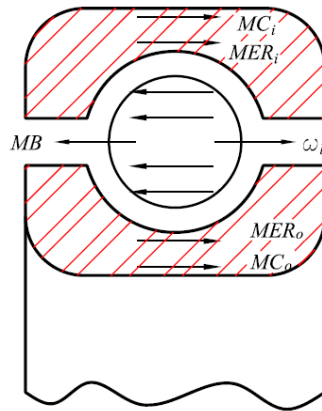
Figure 2.   Moments acting on a ball and the two races of a ball bearing system.
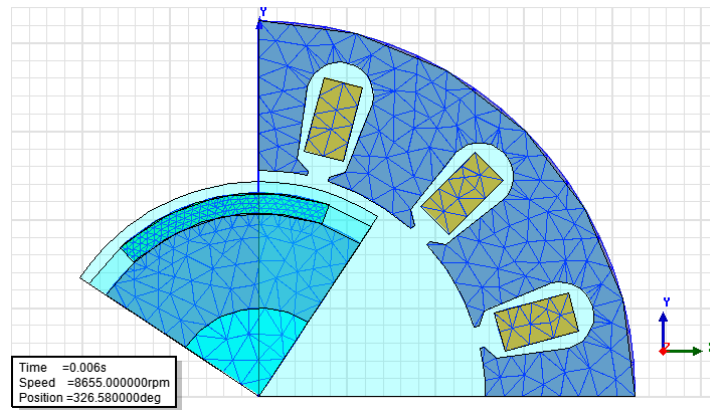
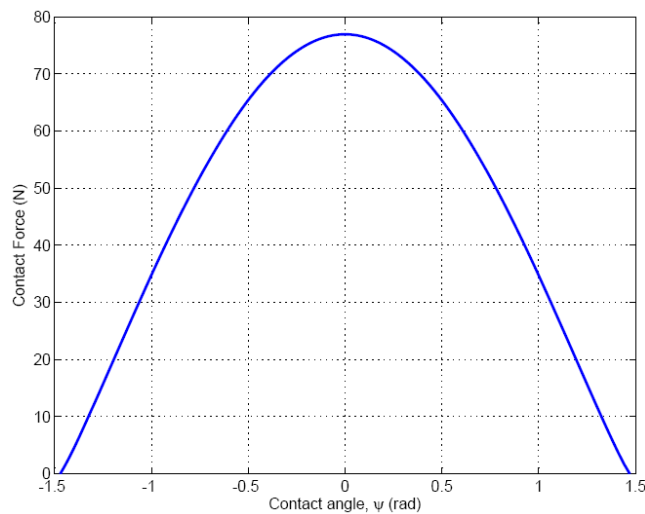Figure 3. 2D FEA mesh in Ansoft MAXWELL.

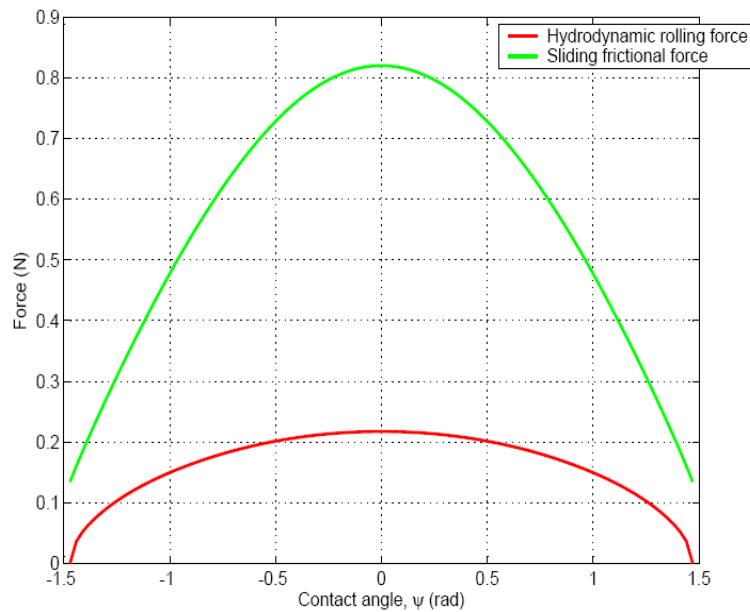Figure 4. Load distribution on a rolling element bearing, for a radial force of 200N.

Figure 5. Hydrodynamic and sliding friction forces on a rolling element at a radial load of 200N and a speed of 6000rpm.
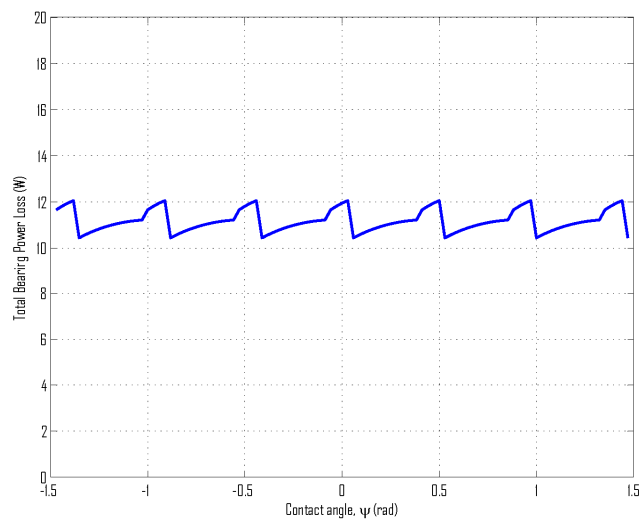

Figure 6. Bearing friction loss across the loading zone (for a radial load of 80N and rotational speed of 8000rpm).
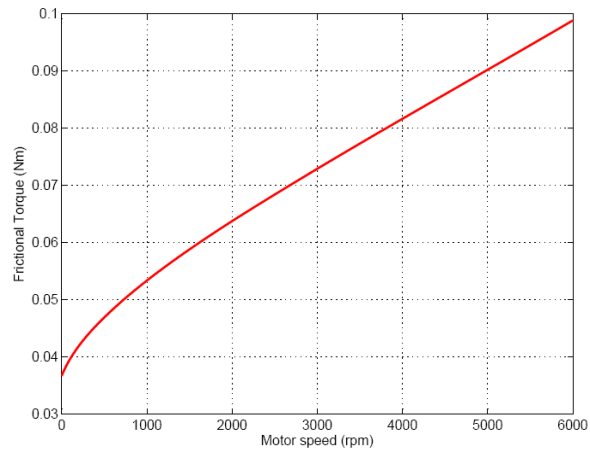
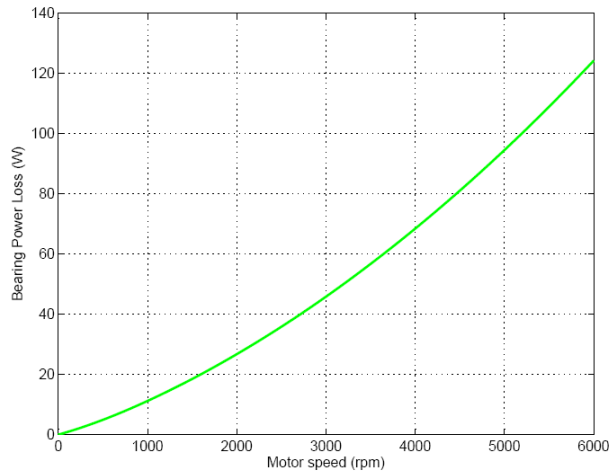Figure 7. Variation of bearing frictional torque with speed for constant radial load of 200N.

Figure 8. Variation of bearing frictional power loss with speed for constant radial load of 200N.
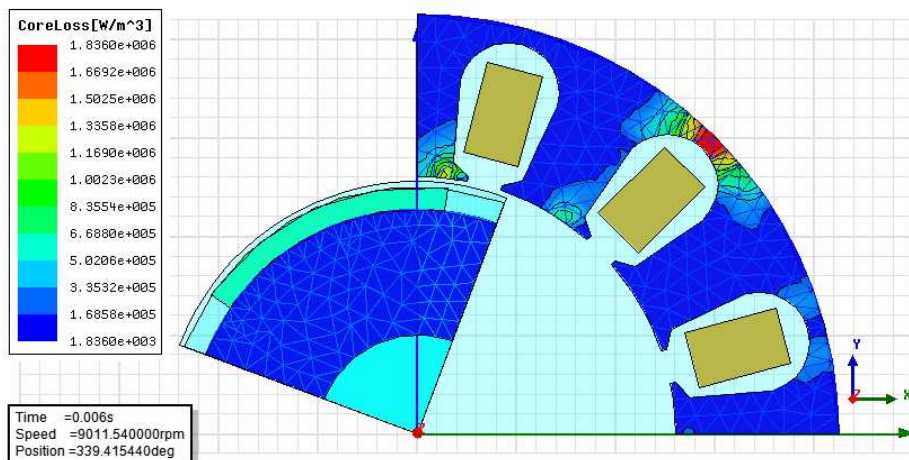

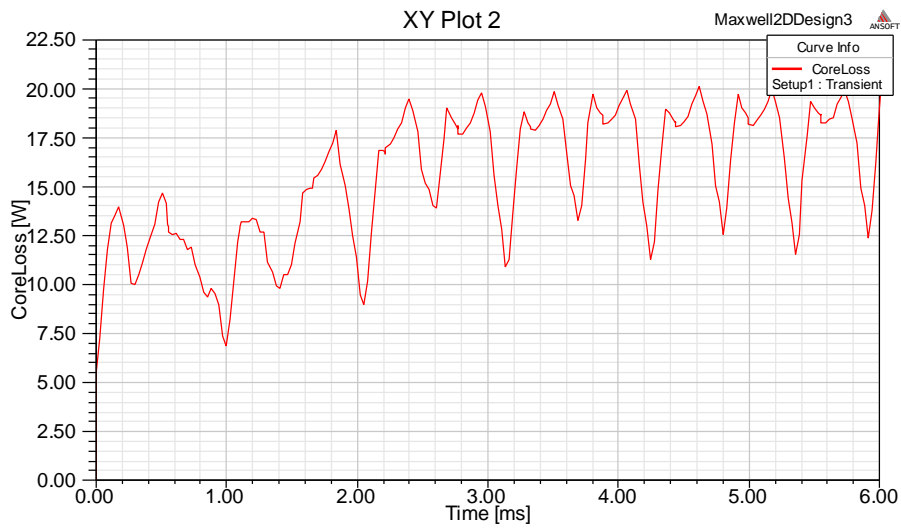Figure 9. Contours of coreloss in a BLDC motor, obtained from MAXWELL simulations.
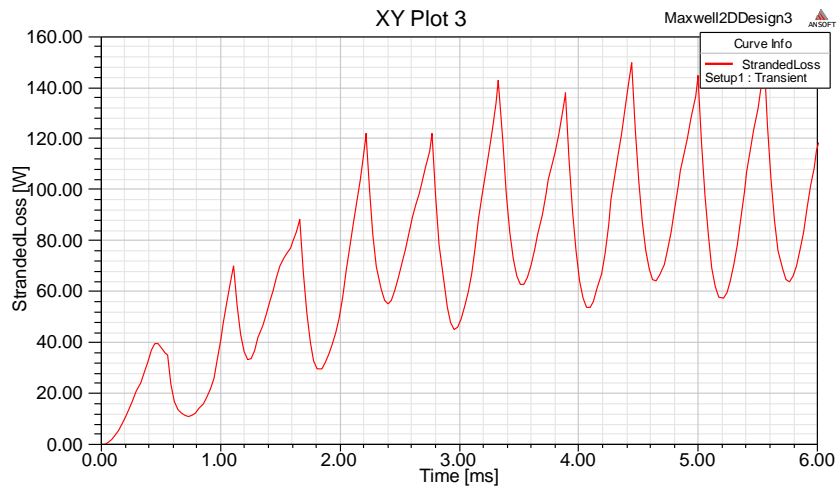
Figure 10. Transient stator core loss.

Figure 11. Transient stranded copper loss.

This academic article was published by The International Institute for Science, Technology and Education (IISTE). The IISTE is a pioneer in the Open Access Publishing service based in the U.S. and Europe. The aim of the institute is Accelerating Global Knowledge Sharing.

More information about the publisher can be found in the IISTE's homepage:
http://www.iiste.org

The IISTE is currently hosting more than 30 peer-reviewed academic journals and collaborating with academic institutions around the world. **Prospective authors of IISTE journals can find the submission instruction on the following page:**
http://www.iiste.org/Journals/

The IISTE editorial team promises to the review and publish all the qualified submissions in a fast manner. All the journals articles are available online to the readers all over the world without financial, legal, or technical barriers other than those inseparable from gaining access to the internet itself. Printed version of the journals is also available upon request of readers and authors.

IISTE Knowledge Sharing Partners

EBSCO, Index Copernicus, Ulrich's Periodicals Directory, JournalTOCS, PKP Open Archives Harvester, Bielefeld Academic Search Engine, Elektronische Zeitschriftenbibliothek EZB, Open J-Gate, OCLC WorldCat, Universe Digtial Library , NewJour, Google Scholar